Chapter 9
Modelling of Shock-Accelerated Gamma-Ray Events

Alexandr Afanasiev, Angels Aran, Rami Vainio, Alexis Rouillard, Pietro Zucca, David Lario, Suvi Barcewicz, Robert Siipola, Jens Pomoell, Blai Sanahuja, and Olga E. Malandraki

Abstract Solar γ-ray events recently detected by the *Fermi*/LAT instrument at energies above 100 MeV have presented a puzzle for solar physicists as many of such events were observed lasting for many hours after the associated flare/coronal mass ejection (CME) eruption. Data analyses suggest the γ-ray emission originate from decay of pions produced mainly by interactions of high-energy protons deep in the chromosphere. Whether those protons are accelerated in the associated flare or in the CME-driven shock has been under active discussion. In this chapter, we present some modelling efforts aimed at testing the shock acceleration hypothesis.

A. Afanasiev (✉) • R. Vainio • S. Barcewicz • R. Siipola
Department of Physics and Astronomy, University of Turku, 20014 Turku, Finland
e-mail: alexandr.afanasiev@utu.fi; rami.vainio@utu.fi; t09susaa@utu.fi; roamsi@utu.fi

A. Aran • B. Sanahuja
Departament de Física Quàntica i Astrofísica, Institut de Ciències del Cosmos (ICCUB), Universitat de Barcelona, Barcelona, Spain
e-mail: angels.aran@fqa.ub.edu; blai.sanahuja@ub.edu

A. Rouillard
Institut de Recherche en Astrophysique et Planétologie, Université de Toulouse, Toulouse, France
e-mail: arouillard@irap.omp.eu

P. Zucca
LESIA - Observatoire de Paris, CNRS, 92190 Meudon, France
e-mail: pietro.zucca@obspm.fr

D. Lario
Applied Physics Laboratory, Johns Hopkins University, Laurel, MD 20723, USA
e-mail: david.lario@jhuapl.edu

J. Pomoell
Department of Physics, University of Helsinki, 00014 Helsinki, Finland
e-mail: jens.pomoell@helsinki.fi

O.E. Malandraki
National Observatory of Athens, IAASARS, Athens, Greece
e-mail: omaland@astro.noa.gr

O.E. Malandraki, N.B. Crosby (eds.), *Solar Particle Radiation Storms Forecasting and Analysis, The HESPERIA HORIZON 2020 Project and Beyond*, Astrophysics and Space Science Library 444, DOI 10.1007/978-3-319-60051-2_9

We address two γ-ray events: 2012 January 23 and 2012 May 17 and approach the problem by, first, simulating the proton acceleration at the shock and, second, simulating their transport back to the Sun.

9.1 Introduction

The novel γ-ray observations by the Large Area Telescope (LAT) on the *Fermi* γ-ray Space Telescope spacecraft (Atwood et al. 2009), taken in a systematic way at unprecedented high energies, have presented a puzzle to the solar energetic particle (SEP) research community. More than two dozen >100 MeV γ-ray events were observed between 2008 and 2016 (see Chap. 8), many of which have properties that challenge the traditional idea that high-energy (>300 MeV) protons needed for the production of the γ-rays, via the pion-decay process deep in the chromosphere, are accelerated in solar flares (Ackermann et al. 2014). Specifically, the *Fermi*/LAT observations indicate that particles are precipitating to the solar atmosphere for up to a day after the impulsive phase of the flare, which is difficult to reconcile with a model of impulsive acceleration followed by particle trapping in the coronal magnetic field. On the other hand, coronal mass ejection (CME) driven shock waves can emit protons with energies above 300 MeV for several hours after the onset of the associated solar eruption as observed at 1 AU (e.g., the 2012 May 17 SEP event, see Chap. 8). Therefore, as an alternative view on the genesis of the long-duration γ-ray events, shock acceleration needs to be considered.

One of the challenges of the shock-acceleration hypothesis is that the SEP events observed in connection with the *Fermi*/LAT γ-ray events are not always very large, nor do they extend to very high energies when observed at 1 AU (see Chap. 8). Therefore, one of the key aspects to understand about these events is the spatial distribution of the accelerated particles at the CME-driven shock wave as well as the relation between interplanetary and interacting protons. Several factors contribute to this relation: (1) In-situ observations are local, i.e., performed in a particular interplanetary flux tube, whereas the observed high-energy γ-rays are produced over an extended emission region involving contributions from different field lines. (2) The energy spectrum of the particles accelerated at the shock is modified by transport effects when the particles propagate both downstream and upstream to reach the Sun and 1 AU. (3) Particles can modify their own transport conditions upstream of the shock due to amplification of Alfvén waves, so the fluxes observed at 1 AU can be partially decoupled from the fluxes at the shock. (4) Compressive and stochastic acceleration in the downstream region close to the CME can modify the spectrum of particles propagating toward the Sun.

We tackle the problem by conducting simulations of acceleration of protons in the shock and of their transport to 1 AU and back to the Sun for two long-duration γ-ray events: 2012 January 23 and 2012 May 17, of which the latter is associated with a ground level enhancement (GLE) of SEPs. In what follows, we outline in Sect. 9.2 the modelling techniques applied, then we present simulation results in Sect. 9.3 and their discussion as well as conclusions in Sect. 9.4.

9.2 Model Description

In this section, we outline the Shock-and-Particle (SaP) and Coronal Shock Acceleration (CSA) simulation models used to infer the proton spectrum at the shock and describe in detail the DownStream Propagation (DSP) model developed in the frame of High Energy Solar Particle Events foRecastIng and Analysis (HESPERIA) project and used to simulate proton transport from downstream of the shock to the Sun's surface.

9.2.1 Shock and Particle Model

The Shock-and-Particle (SaP) simulation model allows one to determine the injection rate of energetic particles from a propagating shock, using simulations of the shock propagation and particle transport, combined with the fitting of the simulation results to the observations. The particle injection rate Q at the shock is defined as $Q = \mathrm{d}f(z_\mathrm{s}, E, t)/\mathrm{d}t$, where f is the particle phase-space distribution function and $z_\mathrm{s}(t)$ is the shock position along the magnetic field line, which is, of course, a function of time. In SaP, the Parker spiral magnetic field is assumed. Instead of Q, one can consider the injection rate integrated over the cross-section A of the magnetic tube, $G = QA(z_\mathrm{s})$. See Chap. 4, Pomoell et al. (2015) and Aran et al. (2007) for further details.

9.2.2 Coronal Shock Acceleration Model

The Coronal Shock Acceleration (CSA) model is a Monte Carlo simulation model dealing with acceleration of ions in a coronal shock, taking into account ion-induced generation of Alfvén waves in the solar wind upstream of the shock. CSA simulates evolution of particles and Alfvén waves on a single radial magnetic field line. The shock is treated as a magnetohydrodynamic (MHD) discontinuity, the gas and magnetic compression ratios of which are computed through Rankine-Hugoniot relations, using the shock speed along the field line V_s, the shock-normal angle θ_Bn (the angle between the magnetic field vector $\mathbf{B}$ and the shock normal $\mathbf{n}$) and the ambient solar wind parameters (the plasma density n, the magnetic field B and the temperature T) at the shock position. All these parameters vary as the shock propagates outward from the Sun, which is implemented in CSA by using analytic functions of time or heliocentric distance to describe such variations. The analytic functions are determined by a number of free parameters that have to be provided as input in a simulation (see Afanasiev et al. 2017 for details). For instance, the

variation of the magnetic field strength B with heliocentric distance r is implemented in CSA as

$$B(r) = B_0 \left(\frac{r_\oplus}{r}\right)^2 \left[1 + b_{\mathrm{rf}} \left(\frac{R_\odot}{r}\right)^6\right], \tag{9.1}$$

where $R_\odot$ is the solar radius, $r_\oplus = 1$ AU, and B_0 and b_{rf} are free parameters. The parameter b_{rf} accounts for a super-radial expansion of the associated radial magnetic flux tube close to the solar surface. In HESPERIA, the free parameters were determined by fitting the analytic functions used to the data obtained by using techniques of semi-empirical modelling of the shock (see Rouillard et al. 2016).

The treatment of wave-particle interactions in CSA is based on quasi-linear theory, assuming only outward-propagating Alfvén waves, i.e., waves propagating away from the Sun. Particles experience elastic pitch-angle scattering in the wave frame, which is governed by the quasi-linear pitch-angle diffusion coefficient:

$$D_{\mu\mu} = \frac{\pi}{4}\Omega \frac{f_{\mathrm{res}} P(f_{\mathrm{res}})}{B^2} \left(1 - \mu^2\right), \tag{9.2}$$

where $P(f)$ is the wave power spectrum, $f_{\mathrm{res}} = \Omega V/(2\pi v)$ is the resonant wave frequency, v and μ are the particle speed and pitch-angle cosine as measured in the wave-rest frame, V is the Alfvén wave propagation speed as measured in the solar-fixed frame and Ω is the ion cyclotron frequency. The expression given for the resonance frequency f_{res} represents a simplified (pitch-angle-independent) resonance condition of particle pitch-angle scattering (see, e.g. Afanasiev et al. 2015). If considered in other reference frames, in particular in the plasma frame, pitch-angle scattering leads to the energy exchange between particles and waves. Pitch-angle scattering of particles off outward-propagating waves, as viewed in the plasma frame, can give rise to growth of waves. After a series of approximations (Vainio 2003), the wave growth is given as

$$\Gamma(f_{\mathrm{res}}) = \frac{\pi}{2}\Omega \frac{p_{\mathrm{res}} S(r, p_{\mathrm{res}}, t)}{n V_{\mathrm{A}}}, \tag{9.3}$$

where $S(r,p,t) = 2\pi \int_{-1}^{+1} p^2 \mu v f(r,p,t) \mathrm{d}\mu$ is the particle streaming, p_{res} is the resonant particle momentum corresponding to the resonance frequency f_{res}, n is the proton density and V_{A} is the Alfvén speed.

Particles are followed in the guiding-center approximation in the shock's upstream. The seed particle population is modelled by a kappa distribution in speed with an exponential cutoff energy E_0. The spatial distribution of seed particles is parameterised as $n_{\mathrm{seed}} = \epsilon n$, where n_{seed} is the density of seed particles and ϵ is the injection parameter. Particle injection at the shock as well as particle-shock interactions are modelled by testing particles hitting the shock from the upstream for reflection/transmission from/through the shock front and for their transport back

to the upstream, if transmitted. Alfvén waves are followed in the Wentzel-Kramers-Brillouin (WKB) approximation, with an additional diffusion term in frequency accounting for wave energy cascading. For a comprehensive description of CSA see Battarbee (2013).

9.2.3 DownStream Propagation Model

The DownStream Propagation (DSP) model is a Monte Carlo simulation model that has been devised to simulate proton transport from the shock's downstream back to the Sun. It is based on Parker's equation, which assumes quasi-isotropic particle distributions and, hence, diffusive transport:

$$\frac{\partial f}{\partial t} + \mathbf{u} \cdot \nabla f - \frac{1}{3} p (\nabla \cdot \mathbf{u}) \frac{\partial f}{\partial p} = \nabla \cdot (\kappa \cdot \nabla f) \ , \tag{9.4}$$

where $f = \langle \mathrm{d}^6 N / (\mathrm{d}^3 x \, \mathrm{d}^3 p) \rangle$ is the isotropic part of the particle distribution function, $\mathbf{u}$ is the velocity of the background fluid (solar wind plasma) and κ is the diffusion tensor. The second term on the left-hand side describes advection of particles with the solar wind, the third term describes adiabatic cooling due to the solar wind expansion and the right-hand side term describes spatial diffusion of particles. Hence, DSP describes the propagation of particles in the test-particle approximation.

Assuming that particles are confined within a magnetic flux tube, which gives $\kappa = \kappa \mathbf{bb}$ with $\mathbf{b}$ being a unit vector along the magnetic field, and that $\mathbf{u} \,||\, \mathbf{b}$, Parker's equation can be reduced to

$$\frac{\partial f}{\partial t} + u \frac{\partial f}{\partial z} - \frac{1}{3} p \frac{1}{A} \frac{\partial (Au)}{\partial z} \frac{\partial f}{\partial p} = \frac{1}{A} \frac{\partial}{\partial z} \left(A \kappa \frac{\partial f}{\partial z} \right) \ , \tag{9.5}$$

where z is the (curvilinear) coordinate measured from the solar surface along the field and $A(z)$ is the cross-sectional area of the flux tube. Changing to $F = 4\pi p^2 A f$, one can obtain

$$\frac{\partial F}{\partial t} + \frac{\partial}{\partial z} \left[\left(u + \frac{1}{A} \frac{\partial (A\kappa)}{\partial z} \right) F \right] - \frac{\partial}{\partial p} \left(\frac{1}{3} p \frac{1}{A} \frac{\partial (Au)}{\partial z} F \right) = \frac{1}{2} \frac{\partial^2}{\partial z^2} (2\kappa F) \ . \tag{9.6}$$

Equation (9.6) is equivalent to the following set of stochastic differential equations (SDEs):

$$\mathrm{d}z = \left(u + \frac{\kappa}{L} + \frac{\partial \kappa}{\partial z} \right) \mathrm{d}t + \sqrt{2\kappa} \, \mathrm{d}W_t \ , \tag{9.7}$$

$$\mathrm{d}p = -\frac{1}{3} p \left(\frac{u}{L} + \frac{\partial u}{\partial z} \right) \mathrm{d}t \ , \tag{9.8}$$

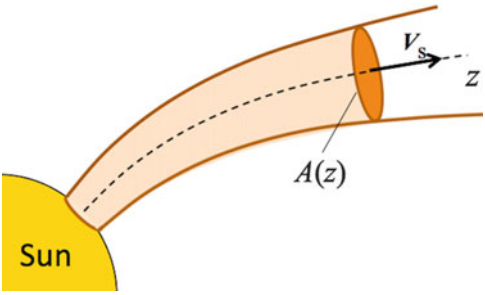

Fig. 9.1 Spatial simulation domain in the DSP model

where $L(z) = A/(\mathrm{d}A/\mathrm{d}z)$ is the focusing length of the magnetic flux tube, $\mathrm{d}W_t$ is a stochastic differential normally distributed with zero mean and variance $\mathrm{d}t$. Note that the term $(\kappa/L)\mathrm{d}t$ in Eq. (9.7) represents the net effect of focusing to a quasi-isotropic particle population (Kocharov 1996). These SDEs are solved for each Monte Carlo particle in the simulation, using the standard explicit Euler-Maruyama method.

The simulation is performed in an expanding 1-D spatial simulation box in the shock's downstream, i.e., the box is confined by the solar surface from one side and by the moving shock front from the other side, and, thus, expands with time along the magnetic field line (Fig. 9.1). For the plasma speed u and the spatial diffusion coefficient κ in the simulation box, the following linear models are adopted:

$$u(z,t) = \frac{u_0 z}{V_s t}\,, \tag{9.9}$$

$$\kappa(z,p,t) = \frac{1}{3}\lambda_0 \frac{p}{m_\mathrm{p}} \frac{V_s t - z}{V_s t}\,, \tag{9.10}$$

where u_0 is the plasma speed immediately behind the shock front and V_s is the shock speed along the field, both measured in the solar-fixed frame, m_p is the proton mass and λ_0 is the particle mean free path at the solar surface. One can see from Eqs. (9.9) and (9.10) that the plasma speed decreases linearly from $u = u_0$ at the shock ($z = V_s t$) to $u = 0$ at the Sun ($z = 0$), and the mean free path recovers from $\lambda = 0$ at the shock to $\lambda = \lambda_0$ at the Sun. Hence the transport of particles from the upstream through the shock is purely advective. On the other hand, the linear dependence of the spatial diffusion coefficient κ on $V_s t - z$ secures that no particles escape from the downstream beyond the shock.

The focusing length L is specified in a form similar to the one that can be derived from Eq. (9.1):

$$L(z) = \frac{1}{2}(R_\odot + z)\left[\left(1 + \frac{z}{R_\odot}\right)^6 + b_\mathrm{f}\right]\left[\left(1 + \frac{z}{R_\odot}\right)^6 + 4b_\mathrm{f}\right]^{-1}\,, \tag{9.11}$$

where b_f is a free parameter.

The initial size of the simulation box is specified by the initial position of the shock z_{s0}. This gives the initial value for time t as $t_0 = z_{s0}/V_s$. The shock speed V_s is assumed constant and $u_0 = V_s(r_c - 1)/r_c$ with r_c being the gas compression ratio taken constant as well.

To be consistent with the chosen form of κ, the amount of particles being injected into the simulation from the shock is determined by the net particle flux to the far downstream. This flux is given by

$$\mathscr{F} = \int \mathrm{d}^3 p \mu v f(p, \mu) = \int \mathrm{d}^3 p' u_2 f'(p') \,, \tag{9.12}$$

where μ is the pitch-angle cosine, v is the particle speed, u_2 is the downstream solar wind speed; the unprimed symbols designate quantities as measured in the shock frame and the primed symbols in the downstream plasma frame. The second expression in Eq. (9.12) is derived under the assumption that the particle pitch-angle distribution as measured in the downstream plasma frame is isotropic. Then, it can be derived to the first order in u_2/c (c is the speed of light in vacuum), taking into account that $\lambda \to 0$ at the shock, that

$$\frac{\mathrm{d}\mathscr{F}}{\mathrm{d}p} = 4\pi u_2 p^2 f_0(p) \,, \tag{9.13}$$

where $f_0(p)$ is the isotropic part of the particle distribution function at the shock (on the upstream side). This equation is used to relate the amount of particles injected to the downstream with the particle intensity at the shock, $j_s = p^2 f_0(p)$, which is the output of CSA simulations. Specifically, the number of particles per unit momentum injected downstream from a source (at the shock) of size $A_s(z)$ in time $\mathrm{d}t$ is determined by

$$\frac{\mathrm{d}N}{\mathrm{d}p} = 4\pi \frac{V_s}{r_c} A_s(z) j_s(t, E) \mathrm{d}t \,. \tag{9.14}$$

In case the particle injection rate $G(t, E)$ is given (output of SaP), the particle intensity at the shock is computed as

$$j_s(t, E) = \frac{p^2}{v} \frac{C \Delta r_g G(t - t_0, E)}{r^2 \cos\psi(r)} \,, \tag{9.15}$$

where v is the particle speed, $C = 3.524$ is a constant determined by the numerical scheme implemented in SaP, Δr_g is the spatial grid size in SaP simulations, r is the heliocentric distance and it is taken into account that in SaP the injection rate G is determined under the assumption of a Parker-spiral upstream magnetic field, i.e., $\cos\psi(r) = [1 + (\Omega_\odot r/u_{sw})^2]^{-1/2}$ with constant solar wind speed u_{sw} ($\Omega_\odot$ is the angular speed of the solar rotation).

The proton injection into the downstream is implemented in the following way. We introduce an injection time step Δt and deposit a certain number of Monte Carlo particles into the simulation box at each Δt. A Monte Carlo particle is a representative of a group of physical particles and is characterised by its weight w. To obtain weights of injected Monte Carlo particles at a given time t_0, we compute values of the spectrum $\mathrm{d}N/\mathrm{d}p$ at the momentum grid using Eq. (9.14) and interpolate those spectral values by power laws between the grid nodes. Then, the weight of a Monte Carlo particle with momentum p between the grid points p_j and p_{j+1} is given by

$$w = \frac{1}{N_{\mathrm{MC}}} \int_{p_j}^{p_{j+1}} \frac{\mathrm{d}N}{\mathrm{d}p}\,\mathrm{d}p, \tag{9.16}$$

where $\mathrm{d}N/\mathrm{d}p \propto p^{-q_j}$ and N_{MC} is the number of Monte Carlo particles assigned to the interval $[p_j, p_{j+1}]$. Note that the particle momentum p is randomly chosen from a p^{-q_j} distribution in this interval and $q_j = -\ln(S_{j+1}/S_j)/\ln(p_{j+1}/p_j)$ with $S_{j(j+1)} = \mathrm{d}N/\mathrm{d}p|_{j(j+1)}$.

The Monte Carlo particles injected at a given time t_0 are placed into a small spatial 1-D volume $\Delta z = u_2 \Delta t$ behind the front, to mimic their advection by the bulk plasma during Δt. Then, each of these particles is propagated by solving the SDEs until it hits the Sun, i.e., precipitates, or up to $t = t_{\max}$. The particle transport time step δt must fulfil the condition $\delta t \ll L^2/\kappa$. Furthermore, the linear dependence of κ on distance from the shock dictates that Monte Carlo particles that might appear in the upstream side during a simulation have to be returned to the downstream side. This requires a reflective boundary condition for particles to be applied at the shock.

During the simulation, Monte Carlo particles that hit the Sun are collected and, based on their momenta, precipitation times and weights, the flux and time-integrated energy spectrum of absorbed protons are calculated. The latter is compared with the proton spectra derived from γ-ray observations.

9.3 Results

The simulations based on the models presented above were conducted for two long-duration >100 MeV γ-ray events occurred on 2012 January 23 and 2012 May 17. These γ-ray events are associated with substantial SEP events as observed at 1 AU (the 2012 May 17 event is also a GLE). The event characteristics are described in Chap. 8 (see also Rouillard et al. 2016). In what follows we first present modelling results for the 2012 May 17 event due to its association with a GLE and then results for the 2012 January 23 event.

9.3.1 2012 May 17 Event

9.3.1.1 Modelling of the SEP Event

We begin with results of the SaP modelling of the accelerated proton population at the shock, which utilises the observations of the shock and SEP event at 1 AU. Figure 9.2 presents results of simulations of the ambient solar wind and shock propagation to the Earth. The solar wind was simulated starting from the onset time of the SEP event. Table 9.1 provides values of the input solar wind parameters at 1.03 $R_\odot$. The input parameters of the shock-driving disturbance are its density $\rho_{\rm cme} = 0.3 \times 10^{-13}$ kg m^{-3}, speed $v_{\rm cme} = 1000$ km s^{-1}, and the shock-front shape parameter $\Delta\phi = 0.5 a_{\rm cme}$ determined by the angular extent $a_{\rm cme}$ of the disturbance (see Pomoell et al. 2015 for details). One can see that the simulations reproduce quite well the average characteristics of the solar wind at 1 AU prior to the shock arrival (note, however, that the temperature is somewhat underestimated) as well as the shock arrival time. At the same time, the observed jumps in the plasma characteristics are reproduced well with some underestimation of the magnetic field increase.

In order to derive the proton injection rate from the shock into the magnetic flux tube connecting the observer with the shock front, we fitted the proton

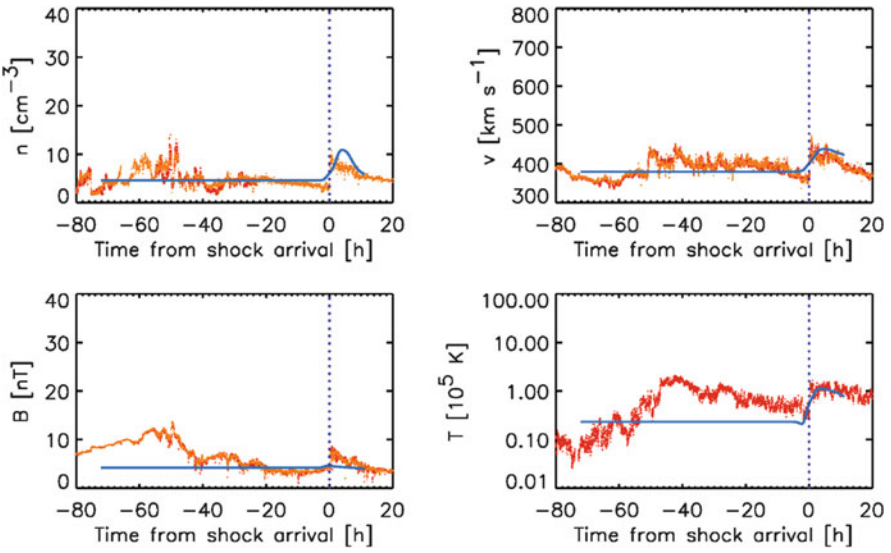

Fig. 9.2 Simulated characteristics of the solar wind (*blue lines*) superposed on the observed characteristics (shown in *orange and red*) before and during the shock arrival at 1 AU for the 2012 May 17 SEP event. Shown are: the plasma density, the solar wind radial velocity, the magnetic field magnitude and the solar wind proton temperature. The temperature was measured by the Wind spacecraft and the other parameters by the ACE spacecraft. Time counts from the time of the interplanetary shock passage by the ACE spacecraft (marked by a *dotted vertical line*)

Table 9.1 Input solar wind parameters used in the SaP simulations of the 2012 January 23 and 2012 May 17 SEP events

Event	ρ_0 (kg/m^3)[a]	T_0 (K)	S_0 (W/m^3)	$\mathscr{L}$ (R$_\odot$)	γ	B_{r0} (T)
Jan 2012	1.169×10^{-13}	1.22×10^6	0.335×10^{-7}	0.735	1.55	-2.15×10^{-4}
May 2012	1.169×10^{-13}	1.18×10^6	0.35×10^{-7}	0.70	1.55	1.26×10^{-4}

[a]The parameters provided are the plasma density ρ_0, temperature T_0 and the radial component of the magnetic field B_{r0} at the heliocentric distance $r_0 = 1.03$ R$_\odot$; S_0 and $\mathscr{L}$ are the coronal heating function parameters (Pomoell et al. 2015); and γ is the adiabatic index.

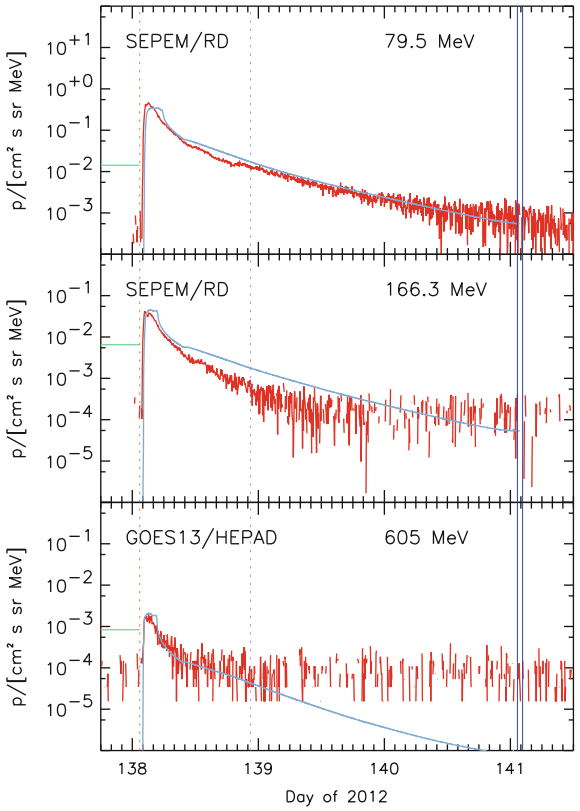

Fig. 9.3 Examples of the intensity-time profiles from the SEPEM reference data and the GOES/HEPAD detector (shown in *red*) with superposed fits (*light blue lines*). The *short green horizontal lines* indicate the pre-event background intensities that have been subtracted from the measured intensities. The *two solid blue vertical lines* indicate the times of the shock arrival at the ACE and GOES spacecraft positions. The *dotted orange vertical line* indicates the onset of the associated X-ray flare and the *dotted purple line* indicates the time of a change in the interplanetary magnetic field direction

intensity-time profiles provided by the ACE/EPAM instrument (in the energy range 0.59–4.8 MeV), SEPEM reference data (Jiggens et al. 2012) (6–166.3 MeV) and GOES/HEPAD detector (330–700 MeV). The fitting was performed using SaP particle transport simulations, following the method described in Pomoell et al. (2015). Figure 9.3 shows examples of the fitted intensity-time profiles for several high-energy channels. Note that when performing the fitting, we focused on the first several hours of the event as the corresponding γ-ray event lasted for about 2 h.

Figure 9.4 shows the proton injection rates $G(t)$ resulting from the fitting of the intensity-time profiles at selected energies. The obtained injection rates were used

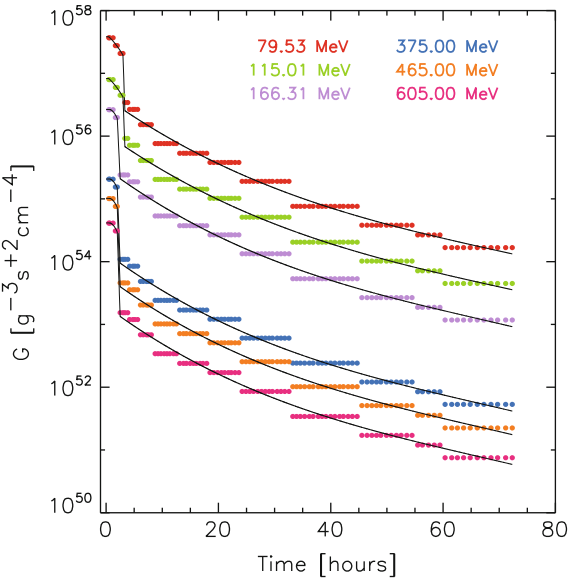

Fig. 9.4 Temporal evolution of the proton injection rate G at high energies. *Black lines* represent polynomial fits to the simulated G functions

as input for the DSP simulations. The simulations reveal that the injection rate at high energies drops by more than one order of magnitude several hours after the X-ray flare onset, which agrees with rather short duration of the associated γ-ray event ($\sim$2 h).

9.3.1.2 Simulations of Proton Acceleration at the Shock

To carry out the CSA simulations of proton acceleration at the shock in this event, we utilised the ambient plasma and shock parameters derived from the semi-empirical modelling of the shock (Rouillard et al. 2016). Those parameters are the plasma density n, the magnetic field strength B, the shock speed V_s and the shock-normal angle θ_{Bn}, which were determined along individual magnetic field lines. The parameters were fitted by the analytic functions of time/distance implemented in CSA (Afanasiev et al. 2017). Figure 9.5 shows an example of the data obtained for a single field line, superposed by the corresponding fits. In total, the data for over 100 field lines were available and fitted. Among the field lines possessing good-quality fits, nine were chosen for simulations with CSA.

The detailed analysis of the simulation results presented in Afanasiev et al. (2017) reveals that the parameter mainly controlling the acceleration efficiency is the Alfvénic Mach number of the shock. Figure 9.6 shows examples of the evolution of the Alfvénic Mach number of the propagating shock for three different magnetic field lines and simulated proton energy spectra at the shock, corresponding to these field lines, obtained at $t = 1000$ s. The simulated spectra (for one of the simulated field lines) were then used as the other input for the DSP simulations.

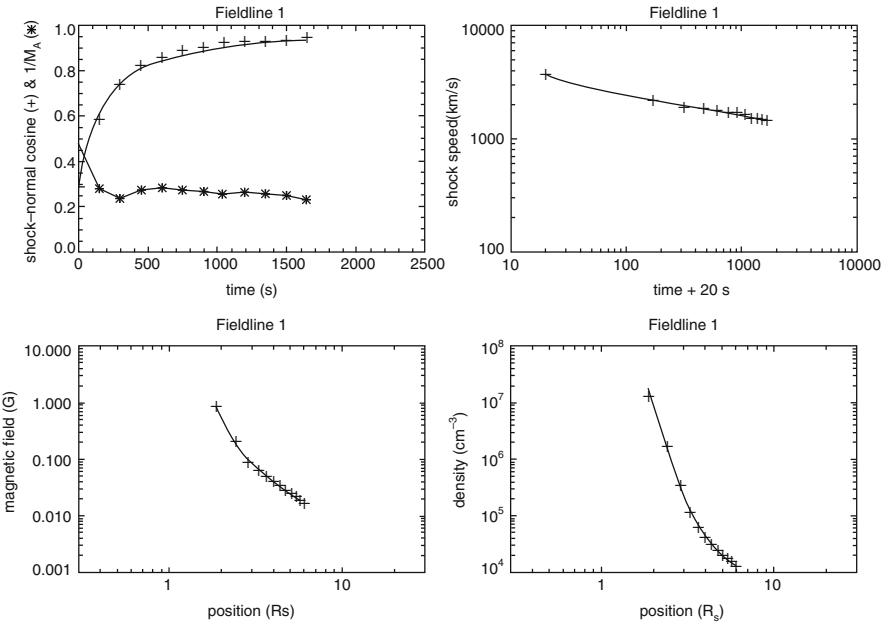

Fig. 9.5 Example data set obtained with the semi-empirical shock modelling approach in the 2012 May 17 event, plotted together with the corresponding fits. The *upper left panel* shows the shock-normal cosine $\cos\theta_{\mathrm{Bn}}$ ("plus" symbols) and the inverse Alfvénic Mach number M_{A}^{-1} (asterisks) vs. time; the *upper right panel* shows the shock speed V_{s} along the magnetic field line vs. time. Note that time is counted from the moment when $M_{\mathrm{A}} > 1.5$. The *bottom left panel* shows the magnetic field magnitude B vs. radial shock position and the *bottom right panel* shows plasma density n vs. radial shock position

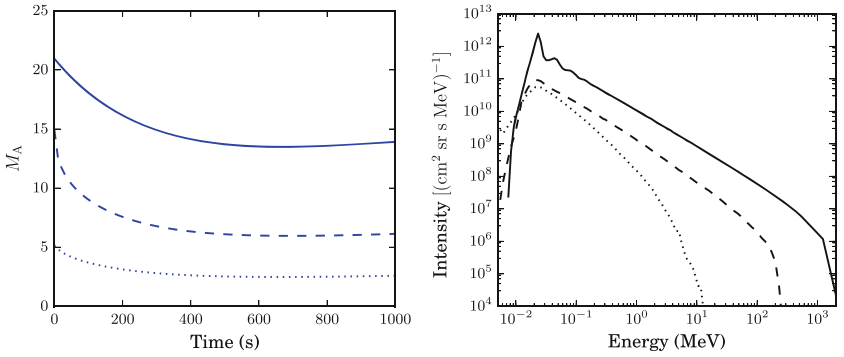

Fig. 9.6 Alfvénic Mach number of the shock versus simulation time for three different magnetic field lines (*left panel*) and corresponding proton energy spectra at the shock at $t = 1000$ s, resulting from CSA simulations (*right panel*). Note the correspondence between the Alfvénic Mach number and the spectral cutoff energy

9.3.1.3 Modelling of the Proton Transport Back to the Sun

The proton transport back to the Sun was simulated with the DSP model, assuming a radial magnetic field in the shock's downstream. The particle source size at the shock was modelled as $A_s(z) = (R_\odot + z)^2\Omega_0$. The parameter Ω_0, which can be interpreted as the global angular size of the shock, was taken to be 1 steradian. In fact, the realistic effective source size should be smaller because of the substantial difference in the particle acceleration efficiency along different field lines, as revealed by the CSA simulations for this event. We took this into account by considering an additional parameter, so-called filling factor, $a_{\rm fill}$ that is the relative fraction of field lines at which high-energy, γ-ray-productive, protons can be produced. Based on the ascertained dependence between the particle acceleration efficiency and the Alfvénic Mach number magnitude, and available data on >100 individual field lines, we estimated that $a_{\rm fill} = 0.1$. To compare the proton spectra resulting from the DSP simulations with the proton spectrum obtained from the *Fermi*/LAT observation, we multiply the simulated spectra by $a_{\rm fill}$. The parameters of the observationally-derived spectrum (the total number of >500 MeV protons and the power-law spectral index of >300 MeV protons) were kindly provided to us by G. Share (see Chap. 8 for references). The other DSP model parameters were taken to be $z_{s0} = 1.6\,R_\odot(1.15\,R_\odot)$, in the case of CSA(SaP) input, $V_s = 1510$ km s^{-1}, $r_c = 3.6$ and $u_{sw} = 387$ km s^{-1}.

The DSP simulations were conducted for a set of values for the downstream transport parameters λ_0 and b_f. The resulting (integrated over the duration of the γ-ray emission; i.e., 2 h) energy spectra of protons hitting the Sun are presented in Fig. 9.7 along with the shock-injected spectrum and the observationally-derived

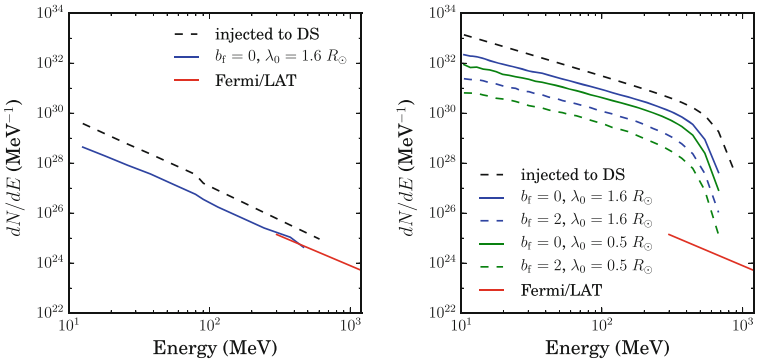

Fig. 9.7 Time-integrated energy spectra of protons precipitated at the Sun, resulting from DSP simulations using the results of SaP (*left panel*) and CSA simulations (*right panel*) for the 2012 May 17 event. The spectra are shown by *blue and green lines* with the corresponding DSP model parameters indicated. The integration time is 2 h, which is approximately the duration of the >100 MeV γ-ray event. Also shown are the time-integrated spectrum of protons injected by the shock to the downstream (*black dashed line*) and the spectrum of interacting protons derived from the *Fermi*/LAT observation (*red line*)

spectrum of interacting >300 MeV protons. It can be calculated that the number of >500 MeV protons injected from the shock in the CSA+DSP simulation exceeds by more than 10^4 the corresponding number of protons derived from the observation. On the other hand, the number of absorbed high-energy protons is sensitive to the transport parameters. In particular, it can be easily reduced by increasing the parameter b_f controlling the focusing length, which enhances proton mirroring from the flux tube base and adiabatic cooling, in accord with Eqs. (9.7) and (9.8). Note also that the DSP model completely neglects the possibility for particles in the downstream side of the shock to escape to the upstream side. This process, if taken into account, should decrease the number of absorbed particles as well.

In contrast, the spectrum of shock-injected protons obtained from the SaP+DSP simulation and the absorbed spectrum corresponding to $b_f = 0$ (radial flux tube) are in good correspondence with the observed spectrum. However, it should be noted that this correspondence holds only for rather idealistic conditions of the DSP model (no particle escape to the upstream) and one can expect a lack of high-energy protons in the simulations, if a more realistic downstream transport model is considered. The possible reasons of this result are discussed in Sect. 9.4.

9.3.2 2012 January 23 Event

9.3.2.1 Modelling of the SEP Event

The results of simulations of the ambient solar wind and shock propagation to 1 AU are shown in Fig. 9.8. The input parameters describing the initial shock-driven disturbance in this case are $\rho_{cme} = 0.3 \times 10^{-13}$ kg m^{-3}, $v_{cme} = 1650$ km s^{-1}, and $\Delta\phi = 0.25 a_{cme}$ (see also Table 9.1 for the initial solar wind parameters). Like for the 2012 May 17 event, the modelling reproduces well the average characteristics of the solar wind at 1 AU prior to the shock arrival and the shock arrival time. The observed jump in the magnetic field magnitude is reproduced well too, but the jumps in the density, the solar wind speed and the temperature are somewhat overestimated. Note that due to the data gap in the ACE data, the value of the average temperature (2.5×10^4 K) in the upstream region has been taken from the plot provided by the IP shocks data base of the University of Helsinki,[1] based on the WIND data. A similar value is estimated by the CfA interplanetary shock list.[2]

Like for the previous event, we fitted the observed intensity-time profiles provided by the ACE/EPAM instrument and the SEPEM reference data (Jiggens et al. 2012). The proton enhancements observed in this event by GOES/HEPAD in the high-energy channels ranging from 330 to 700 MeV are weak. From Fig. 9.9, it can be seen that already at 166.3 MeV the background-subtracted enhancement is lower than the background level itself. For this reason, instead of fitting the observed

[1] http://ipshocks.fi/database.

[2] https://www.cfa.harvard.edu/shocks.

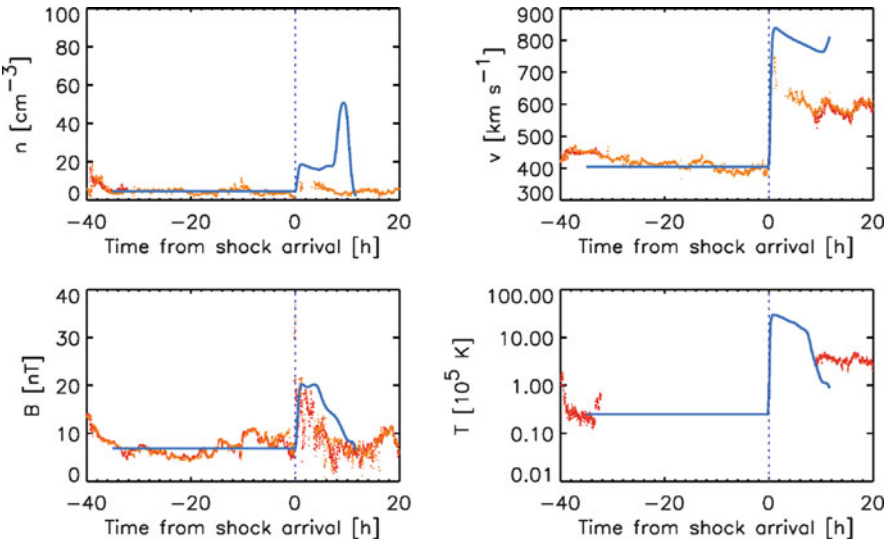

Fig. 9.8 Same as in Fig. 9.2, but for the 2012 January 23 event

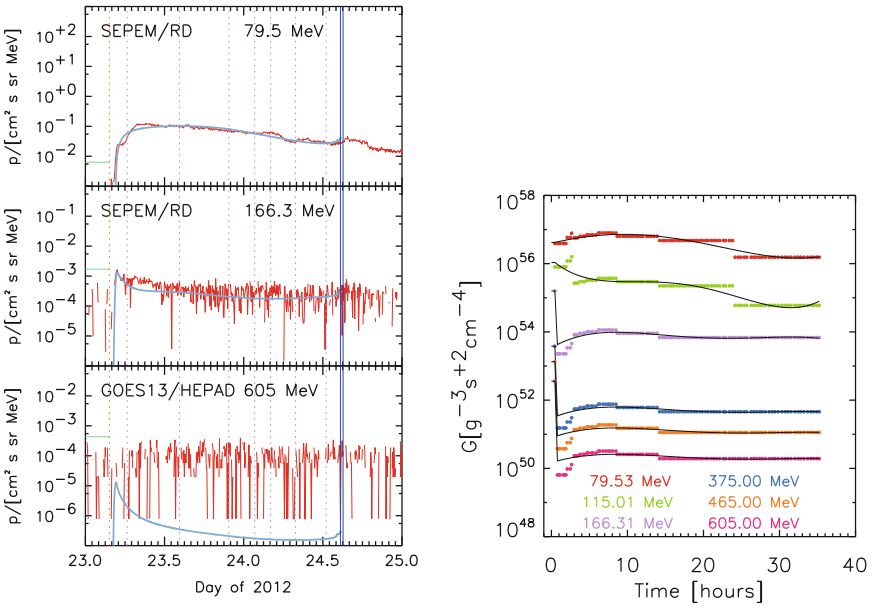

Fig. 9.9 *Left panel*: Examples of the observed proton intensity-time profiles (*in red*) with superposed fits/synthetic profiles (*light blue lines*) for the 2012 January 23 SEP event. The *short green horizontal lines* indicate the pre-event background intensities that have been subtracted from the measured intensities. The meaning of the *other lines* is the same as in Fig. 9.3. *Right panel*: Temporal evolution of the proton injection rate G at high energies. *Black lines* are polynomial fits to the simulated G functions

intensities, we computed synthetic intensity-time profiles for the GOES/HEPAD energy channels by extrapolating the particle injection rate $G(t, E)$ from the highest energies in the SEPEM reference dataset. Such a profile is shown in Fig. 9.9 at 605 MeV. Figure 9.9, right panel shows the proton injection rate resulting from the SaP simulations of this SEP event.

9.3.2.2 Simulation of Proton Acceleration at the Shock

To conduct CSA simulations of proton acceleration at the shock in the same fashion as it was done for the 2012 May 17 event, we used white-light (WL) images of the corona from SOHO and STEREO A and B and the Potential Field Source Surface (PFSS) modelling of the magnetic field. The WL images were fitted using a spherical representation for the CME. This allowed us to obtain the magnetic field, the shock speed and the shock-normal angle along different field lines (Fig. 9.10). As concerns the plasma density, we used the following representation:

$$n(r) = n_2 \left(\frac{r_\oplus}{r}\right)^2 + n_8 \left(\frac{R_\odot}{r}\right)^8, \tag{9.17}$$

with $n_2 = 10\ \mathrm{cm}^{-3}$ and $n_8 = 8 \times 10^8\ \mathrm{cm}^{-3}$. Since the plasma density was not constrained using the real observations, we performed a CSA simulation only for one magnetic field line. The simulation showed a typical buildup of the proton energy with time and formation of a power-law energy spectrum with a roll-over, similar to the spectra presented in Fig. 9.6. The maximum proton energy at the shock attained the value ~1 GeV at $t = 1130$ s after the start of the simulation, but then was decreasing and reached ~500 MeV at $t = 2000$ s.

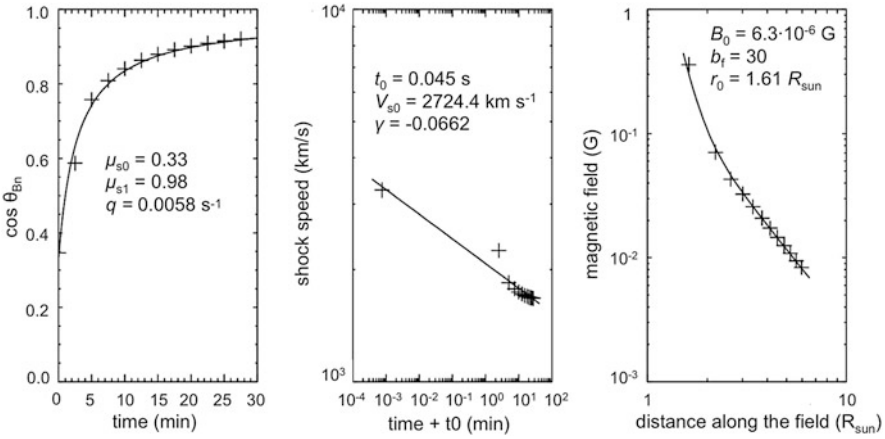

Fig. 9.10 The shock-normal cosine μ_s, the shock speed along the field line V_s and the magnetic field B with the fits superimposed for a selected magnetic field line

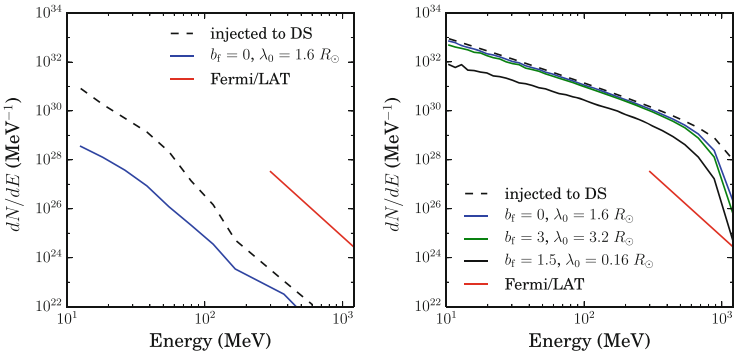

Fig. 9.11 Time-integrated energy spectra of protons precipitated at the Sun, resulting from DSP simulations using the results of SaP (*left panel*) and CSA simulations (*right panel*) for the 2012 January 23 event. The spectra are shown by *blue and green lines* with the corresponding DSP model parameters indicated. The integration time is 6 h. Also shown are the time-integrated spectrum of protons injected by the shock to the downstream (*black dashed line*) and the proton spectra obtained from the *Fermi*/LAT observation (*red line*)

9.3.2.3 Modelling of the Proton Transport Back to the Sun

Similar to the DSP modelling for the 2012 May 17 event, we assumed a radial magnetic field in the shock's downstream and $A_s(z) = (R_\odot + z)^2\Omega_0$ was taken for the particle source at the shock. The model parameters were taken to be $z_{s0} = 0.6\,R_\odot(3.1\,R_\odot)$ in the case of CSA(SaP) input, $V_s = 1450$ km s^{-1}, $r_c = 3.7$, $u_{sw} = 414$ km s^{-1}, $\Omega_0 = 1$ sr, and $a_{fill} = 0.1$.

Figure 9.11 shows the simulated spectra of protons absorbed at the Sun together with the shock-injected spectrum and the proton spectrum derived from the *Fermi*/LAT observation of >100 MeV γ-photons. Similar to the simulation for the 2012 May 17 event, in the CSA+DSP simulation, there is a substantial excess of shock-injected protons as compared to the number of interacted protons derived from the observation. In contrast, there is a lack of shock-injected protons against the observed number in the SaP+DSP simulation.

9.4 Discussion and Conclusions

We have modelled particle acceleration at coronal shocks driven by CMEs and proton transport from the shock to both the Sun and the far upstream region (towards the 1-AU observer). The purpose of our study is to find out, whether shock-accelerated protons streaming back from the shock could be responsible for the long-duration γ-ray events observed by *Fermi*/LAT. We simulated the shock propagation from the Sun to 1 AU using a two-dimensional MHD model. We also employed the empirical models of the CME-driven pressure front propagation,

which allowed us to assess the early evolution of the shock in a system that does not possess the symmetries assumed in the MHD model.

Our results show that the efficiency of particle acceleration crucially depends on the modelled properties of the shock in the corona. Conditions on different field lines vary very much and while the shock on some field lines is able to produce a relativistic particle event, it fails to do so on others. The most important factor governing the acceleration efficiency in our study was the Alfvénic Mach number of the shock: the higher the Alfvénic Mach number, the more likely the shock to accelerate protons to relativistic energies (Afanasiev et al. 2017).

In our simulations, we focused on two events that differ in one important aspect: one of them (2012 May 17) is a GLE and the other one is not. Both of the events are associated with long-duration γ-ray events, which might seem contradictory, but actually is not. In the light of our simulations, there are two possible explanations for this. Firstly, as the particle acceleration efficiency at the shock varies a lot from one flux tube to another, the 1-AU proton event does not necessarily correspond to the best acceleration conditions on the shock surface. Thus, we may well observe a long-duration (pion-decay) γ-ray event due to shock-accelerated protons without a clear increase observed at 1 AU at energies required for pion production at the Sun. The Earth-based observer sees but a small fraction of the complete picture. The other, more subtle explanation deals with the strength of the turbulence in the foreshock region of the coronal shock. The CSA simulations show that the foreshock is extremely turbulent near the Sun, traps a large fraction of particles (almost all) in its vicinity and allows only a minor fraction to escape. While the SaP model contains the possibility to use enhanced foreshock turbulence, it is tuned to reproduce the observations when the shock is detected in situ. Therefore, the source function deduced from the 1-AU observation represents more the fraction of particles that can escape upstream than the fraction that can be transported downstream from the shock. The large discrepancy between the CSA and SaP modelled spectra of precipitated particles is, thus, partly explained by this effect, as well. Furthermore, these explanations shed light on the tendency to get lower numbers of precipitated $>$300 MeV protons in the SaP+DSP simulations (especially for the 2012 January 23 event), as compared to the observations.

The transport model we employ for the downstream region has several important simplifications in it. Firstly, it employs a shock completely opaque to protons and, thus, allows downstream-advected particles to reside in the region between the shock and the Sun for as long as they get precipitated. The only loss process we employ is adiabatic cooling of the distribution, when the region between the shock and the Sun expands. On the other hand, we do not include any downstream re-acceleration processes, which could also be important and would act in the opposite direction, helping particles to overcome adiabatic energy losses. Such processes include downstream stochastic acceleration (see, e.g., Afanasiev et al. 2014) and compressive acceleration in the highly-compressed regions close to the CME core (Kozarev et al. 2013). Therefore, we do not regard our model to be overly optimistic about the prospect of letting shock-accelerated protons precipitate over large time scales.

Regarding the CSA model, one important reservation has to be made: the model makes a simplification to the quasi-linear resonance condition between particles and scattering Alfvén waves, $k_{\mathrm{res}} = 2\pi f_{\mathrm{res}}/V = B/(R\mu)$, neglecting the dependence of resonant wave number k_{res} on particle pitch-angle cosine μ (R is the particle rigidity). This simplification, while without proper physical justification, allows one to build the code using the assumption of isotropic scattering, which speeds up the running times easily by a factor of ten over times obtained when treating the resonance condition in full. We have, however, evaluated the effect of this simplification using a local model (Afanasiev et al. 2015), and shown that in parallel coronal shocks the difference between the two models yields about a factor of 2 in the roll-over rigidity obtained from the model. On the other hand, the spectrum in CSA also cuts off much more rapidly than in the model employing the complete resonance condition, so we do not regard this to be a very serious problem in the performed modelling. A more complete global model to be developed in future, however, should take the full resonance condition into account, also since it affects the foreshock spatial structure as well (Afanasiev et al. 2015). We will undertake the development of such a model in future projects.

Another transport process missing from the CSA model is diffusion perpendicular to the mean magnetic field. This process can be implemented in a Monte Carlo simulation, but its inclusion will require to incorporate at least one more spatial dimension in the model. Therefore, also the requirement for particle statistics in CSA will be tremendously increased to avoid statistical noise in the result, as the number of spatial cells in the model will have to be increased by a factor 30–300, depending on the coarseness of the grid in the perpendicular direction. This is still beyond the reach of the present computers with reasonable running times of the code. Fortunately, as perpendicular diffusion cannot occur due to slab-mode waves, the enhanced Alfvénic turbulence in the upstream region is not strengthening the perpendicular diffusion of the particles. However, one would expect the downstream plasma to have much more isotropic turbulence which, then, would lead to the migration of particles from one flux tube to the other while they are on the downstream side of the shock. For an opaque shock, like we have assumed, this is not affecting the acceleration of ions at the shock too much since their fate (scattered back to the shock or transported to the far downstream region with no return) would be decided (almost) instantly, giving the particles very little time to diffuse perpendicular to the mean field. Thus, the first step to take the perpendicular transport into account would have to be performed on the downstream side of the shock.

We note that the total number of >500 MeV protons as simulated by the CSA code is several orders of magnitude larger than the observational value in both of the simulated events. At first, this might seem to be problematic. However, in addition to the caveats about the resonance condition and the downstream transport modelling discussed above, we point out that the CSA model is set up quite favourably for efficient particle acceleration: we use a seed particle population with a relatively hard suprathermal distribution ($\kappa = 2$) in the model, which guarantees an efficient injection to the acceleration process at all obliquity angles of the shock. Using a

thermal population, only, would limit the injection efficiency of the shock especially at obliquity angles greater than $\sim 20^\circ$ quite substantially: according to Battarbee et al. (2013), the injection efficiency in an oblique coronal shock would go down by an order of magnitude if we would use a steeper seed population with $\kappa = 15$. Given all the possible ways to limit the number of precipitating protons in our model, we would regard the result of getting more than enough high-energy protons precipitating at the Sun to be a supporting rather than a countering result for the shock acceleration scenario.

The final shortcoming in the shock models we have employed is their assumption of the open topology of the upstream magnetic fields. Especially if the γ-ray event occurs during a period of closely spaced CMEs, the second one may drive a shock through a set of large closed loop-like or flux-rope structures, which would alter both the shock acceleration properties and, more importantly, the ability of the particles to escape upstream from the shock. In fact, developing codes capable of modelling particle acceleration and transport in more complicated upstream fields than the radial/Archimedean-spiral fields could be listed as one of the most urgent things needing improvement on the way towards physical space-weather modelling capabilities.

One of the most difficult things to estimate is the size of the source of near-relativistic protons in the event. While the 3-D modelling of the shock front can be performed in a relatively accurate and detailed manner, high-resolution density and magnetic-field structure of the corona are crucial for the correct determination of the shock properties and, thus, the total number of interacting protons in the event. Therefore, even a fully global 3-D model of coronal shock evolution and particle acceleration might not capture every detail affecting the total number of relativistic protons in the CME system. In this work, we resorted to estimating numbers based on the filling factor of field lines being capable of facilitating proton acceleration to relativistic energies based on an evaluation of shock properties on a large set of field lines. We believe that such statistical method to estimate the total number of interacting protons is the most efficient way to address the problem.

In conclusion, while a number of simplifications have been introduced in the modelling performed, we have still demonstrated that coronal shock acceleration and subsequent diffusive downstream particle transport is a viable option to explain pion-decay γ-ray events from the Sun observed by *Fermi*/LAT. More elaborated simulation models are needed (especially for the particle transport back to the Sun) but our results serve as a motivation by indicating that the end result of this vast modelling effort can be positive.

References

Ackermann, M., Ajello, M., Albert, A., et al.: Astrophys. J. **787**, 15 (2014). doi:10.1088/0004-637X/787/1/15

Afanasiev, A., Vainio, R., Kocharov, L.: Astrophys. J. **790**, 36 (2014). doi:10.1088/0004-637X/790/1/36

Afanasiev, A., Battarbee, M., Vainio, R.: Astron. Astrophys. **584**, A81 (2015). doi:10.1051/0004-6361/201526750

Afanasiev, A., Vainio, R., Rouillard, A., et al.: Modelling of proton acceleration in application to a ground level enhancement. Astron. Astrophys. (2017, Submitted)

Aran, A., Lario, D., Sanahuja, B., et al.: Astron. Astrophys. **469**, 1123 (2007). doi:10.1051/0004-6361:20077233

Atwood, W.B., Abdo, A.A., Ackermann, M., et al.: Astrophys. J. **697**, 1071 (2009). doi:10.1088/0004-637X/697/2/1071

Battarbee, M.: Acceleration of solar energetic particles in coronal shocks through self-generated turbulence. Ph.D. thesis, University of Turku, Finland (2013). http://urn.fi/URN:ISBN:978-951-29-5574-9

Battarbee, M., Vainio, R., Laitinen, T., Hietala, H.: Astron. Astrophys. **558**, A110 (2013). doi:10.1051/0004-6361/201321348

Jiggens, P.T.A., Gabriel, S.B., Heynderickx, D., et al.: IEEE Trans. Nucl. Sci. **59**, 1066 (2012). doi:110.1109/TNS.2012.2198242

Kocharov, L.G., Torsti, J., Vainio, R., Kovaltsov, G.A.: Sol. Phys. **165**, 205 (1996). doi:10.1007/BF00149100

Kozarev, K.A., Evans, R.M., Schwadron, N.A., et al.: Astrophys. J. **778**, 43 (2013). doi:10.1088/0004-637X/778/1/43

Pomoell, J., Aran, A., Jacobs, C.,et al.: J. Space Weather Space Clim. **5**(27), A12 (2015). doi:10.1051/swsc/2015015

Rouillard, A.P., Plotnikov, I., Pinto, R.F., et al.: Astrophys. J. **833**, 45 (2016). doi:10.3847/1538-4357/833/1/45

Vainio, R.: Astron. Astrophys. **406**, 735 (2003). doi:10.1051/0004-6361:20030822